Human deoxyhypusine hydroxylase, an enzyme involved in regulating cell growth, activates O_2 with a nonheme diiron center

Van V. Vu[a], Joseph P. Emerson[a,1], Marlène Martinho[b], Yeon Sook Kim[c,2], Eckard Münck[b], Myung Hee Park[c,3], and Lawrence Que, Jr.[a,3]

[a]Department of Chemistry and Center for Metals in Biocatalysis, University of Minnesota, 207 Pleasant St. SE, Minneapolis, MN 55455; [b]Department of Chemistry, Carnegie Mellon University, 4400 Fifth Ave., Pittsburgh, PA 15213; and [c]National Institute of Dental and Craniofacial Research, National Institutes of Health, 9000 Rockville Pike, Bethesda, MD 20892

Edited by Edward I. Solomon, Stanford University, Stanford, CA, and approved July 14, 2009 (received for review April 24, 2009)

Deoxyhypusine hydroxylase is the key enzyme in the biosynthesis of hypusine containing eukaryotic translation initiation factor 5A (eIF5A), which plays an essential role in the regulation of cell proliferation. Recombinant human deoxyhypusine hydroxylase (hDOHH) has been reported to have oxygen- and iron-dependent activity, an estimated iron/holoprotein stoichiometry of 2, and a visible band at 630 nm responsible for the blue color of the as-isolated protein. EPR, Mössbauer, and XAS spectroscopic results presented herein provide direct spectroscopic evidence that hDOHH has an antiferromagnetically coupled diiron center with histidines and carboxylates as likely ligands, as suggested by mutagenesis experiments. Resonance Raman experiments show that its blue chromophore arises from a (μ-1,2-peroxo)diiron(III) center that forms in the reaction of the reduced enzyme with O_2, so the peroxo form of hDOHH is unusually stable. Nevertheless we demonstrate that it can carry out the hydroxylation of the deoxyhypusine residue present in the eIF5A substrate. Despite a lack of sequence similarity, hDOHH has a nonheme diiron active site that resembles both in structure and function those found in methane and toluene monooxygenases, bacterial and mammalian ribonucleotide reductases, and stearoyl acyl carrier protein Δ^9-desaturase from plants, suggesting that the oxygen-activating diiron motif is a solution arrived at by convergent evolution. Notably, hDOHH is the only example thus far of a human hydroxylase with such a diiron active site.

DOHH | peroxo intermediate | eIF5A | oxygen activation

Hypusine is an unusual, but highly conserved, amino acid that is found only in the eukaryotic translational initiation factor 5A (eIF5A), a protein that regulates cell proliferation (1, 2). The biosynthesis of eIF5A involves a posttranslational modification of the eIF5A precursor, where a lysine residue is first modified to deoxyhypusine (Dhp) by deoxyhypusine synthase (DHS) and then the nascent Dhp is hydroxylated by deoxyhypusine hydroxylase (DOHH) to form hypusine (Hpu) (Scheme 1) (1, 2). The importance of hypusine and these 2 enzymes has been shown by several studies where depletion of spermidine (3) or inhibition of either DHS or DOHH (4, 5) leads to a decrease of hypusine-containing eIF5A [eIF5A(Hpu)] and inhibition of eukaryotic cell growth. Consequently, these results suggest that eIF5A and DOHH could be promising targets for antitumor (6) and anti-HIV-1 therapies (7).

The hydroxylase activity of recombinant human DOHH (hDOHH) has been shown to depend on Fe(II) and not on any other physiologically relevant divalent metal ion. An estimated iron-to-holoprotein stoichiometry of 2 is observed (8). Sequence examination, homology modeling, and mutagenesis experiments suggest 2 possible iron binding sites consisting of histidine and carboxylate ligands (8, 9). Thus at first glance, hDOHH appears to resemble members of the superfamily of bacterial diiron multicomponent monooxygenases, like methane or toluene monooxygenase,

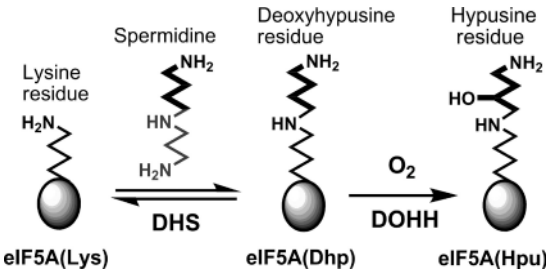

Scheme 1. Biosynthesis of hypusine on eIF5A.

that use nonheme diiron centers to activate dioxygen for the hydroxylation of hydrocarbons (10–12). However there is little sequence similarity between the latter enzymes and DOHH (8).

hDOHH can be overexpressed in *Escherichia coli*, and the enzyme isolated from such cells is blue in color. This chromophore gives rise to 2 absorption features at 320 nm and 630 nm with molar extinction coefficients indicative of ligand-to-metal charge transfer transitions (8). These features resemble those associated with diiron(III)-peroxo intermediates of the hydroxylase component of methane monooxygenase (MMOH) (12), stearoyl-acyl carrier protein Δ^9 desaturase (Δ^9D) (13, 14), the R2 proteins of class I ribonucleotide reductases (R2) (15–19), and the ferroxidase site of frog M ferritin (20, 21). Some of these intermediates have been characterized by resonance Raman spectroscopy and found to exhibit vibrational features typical of a (μ-1,2-peroxo)diiron(III) unit (13, 17, 20).

Here we report direct spectroscopic evidence for a diiron cluster in hDOHH. Interestingly, as-isolated hDOHH is blue in color, and the blue chromophore derives from a peroxo-bridged diiron(III) center that is generated by reaction of the reduced enzyme with oxygen. Comparisons with related diiron(III)-peroxo enzyme intermediates and synthetic complexes shed light on the nature of this active site and augment our understanding of the mechanism of oxygen activation by diiron enzymes.

Author contributions: V.V.V., J.P.E., E.M., M.H.P., and L.Q. designed research; V.V.V., J.P.E., M.M., Y.S.K., and M.H.P. performed research; V.V.V., M.M., and E.M. analyzed data; and V.V.V., E.M., and L.Q. wrote the paper.

The authors declare no conflict of interest.

This article is a PNAS Direct Submission.

[1]Present address: Department of Chemistry, Mississippi State University, Mississippi State, MS 39762.

[2]Present address: Department of Dental Hygiene, Cheongju University, Cheongju, 360–764 Korea.

[3]To whom correspondence may be addressed. E-mail: larryque@umn.edu or mhpark@nih.gov.

This article contains supporting information online at www.pnas.org/cgi/content/full/0904553106/DCSupplemental.

www.pnas.org/cgi/doi/10.1073/pnas.0904553106

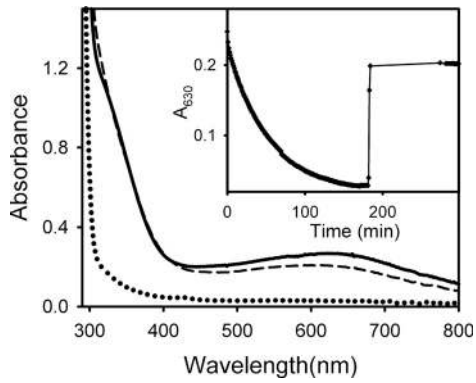

Fig. 1. The UV-Visible spectra of hDOHH at room temperature. Conversion of as-isolated hDOHH (—) by 2.2 equiv. dithionite to reduced hDOHH (···) and its regeneration upon exposure to air after 180 min of anaerobic incubation (– – –). *Inset*: Change of A_{630} with time.

Results

Evidence for an O_2-Activating Diiron Cluster in hDOHH. As-isolated hDOHH is blue in color, with characteristic UV-Visible absorption features at 320 nm and 630 nm (Fig. 1). The features are apparently the result of enzyme-bound iron, as they are absent in the iron-free apoenzyme (8). Upon addition of dithionite, these absorption features decrease slowly over ≈3 h, but rapidly reappear upon exposure of the colorless solution to air, regaining approximately 80% of their initial intensities (Fig. 1 inset). The blue chromophore of hDOHH thus appears to undergo reduction by dithionite and regeneration by exposure to O_2. Reduced hDOHH therefore resembles many oxygen activating nonheme diiron enzymes like RNR R2, MMO, and Δ^9D (12) in its ability to react readily with O_2.

As-isolated hDOHH is EPR silent. Its 4.2 K zero-field Mössbauer spectrum, shown in Fig. 2*A*, consists of a broadened doublet (representing 82% of total Fe) that can be simulated as a superposition of 2 doublets with sharp absorption lines of width 0.27 mm/s (FWHM). The 4 lines can either be assigned to a nested pair, with ΔE_Q (1) = 1.16 (2) mm/s, δ (1) = 0.55 (1) mm/s and ΔE_Q (2) = 0.88 (2) mm/s, δ (2) = 0.58 (1) mm/s, or to a nonnested pair with ΔE_Q (1) = 1.05 (2) mm/s, δ (1) = 0.49 (1) mm/s and ΔE_Q (2) = 0.99 (2) mm/s, δ (2) = 0.63 (1) mm/s. Spectra recorded at 4.2, 20, 50, and 80 K in an 8.0 T applied field show that these doublets belong to an antiferromagnetically coupled pair of high-spin Fe(III) ions, with 50 $cm^{-1} < J < 70$ cm^{-1} (with the convention $H = J \cdot S_1 \cdot S_2$, $S_1 = S_2 = 5/2$). The solid lines in Fig. 2 are spectral simulations obtained with WMOSS option 2Spin. The 8.0 T spectra can be simulated equally well for the nested or the nonnested pair. The sample also contained a high-spin Fe^{3+} contaminant representing ≈18% of the Fe in the sample; a spectrum of this contaminant (Fig. S1) and comments on the fits of Fig. 2 *C* and *D* are presented in the Mössbauer spectroscopy section in *SI Text*.

Protein and Fe concentrations of the sample of Fig. 2*A* were 0.85 mM and 0.56 mM, respectively. Given that ≈18% of the Fe belongs to the Fe(III) contaminant, these concentrations suggest that only 27% of the active sites are occupied by a diiron(III) cluster. Assuming that all absorption at 630 nm can be attributed to the diiron(III) cluster then yields for this sample ε(630 nm) = 2,800 $M^{-1}cm^{-1}$.

Upon treatment with dithionite, the diiron(III) cluster is reduced into the diiron(II) state, $hDOHH_{red}$. This state exhibits 2 doublets characteristic of high-spin Fe(II), with ΔE_Q (1) = 3.26 mm/s, δ (1) = 1.29 mm/s, and ΔE_Q (2) = 2.90 mm/s, δ (2) = 1.29 mm/s (Fig. 2*B*). The sample also contained ≈5% of the original diiron(III) cluster and a high-spin Fe(II) species with ΔE_Q = 2.4 mm/s (≈20%). The percentage of the latter suggests that it represents the reduced form of the Fe(III) contaminant present in the as-isolated sample.

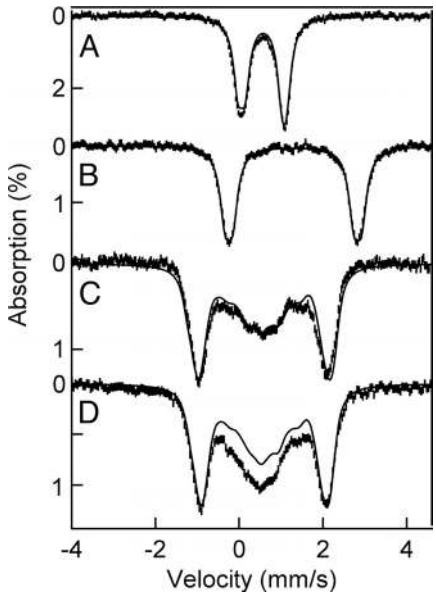

Fig. 2. Mössbauer studies of hDOHH: 4.2 K zero field Mössbauer spectra of as-isolated hDOHH (*A*) and reduced with dithionite (*B*). The solid line in *A* is a simulation assuming 2 nested doublets as described in the text. (*B*) The solid line is a simulation of $hDOHH_{red}$ assuming 2 equally intense doublets representing ≈75% of Fe. Details of data reduction and analyses are given in *SI*. The 8.0 T Mössbauer spectra of as-isolated hDOHH recorded at 4.2 K (*C*) and 50 K (*D*). The solid lines are spectral simulations for an antiferromagnetically coupled diiron(III) center containing 2 high-spin (S = 5/2) Fe(III) sites. For the simulation of the 50-K spectrum we used J = 70 cm^{-1}. At 50 K the central features of the 8.0 T spectrum contain contributions from the mononuclear Fe(III) contaminant (see Mössbauer spectroscopy section in *SI Text*).

We have subtracted the remaining diiron(III) and the Fe(II) contaminant from the raw data to obtain the spectrum of Fig. 2*B* (see Fig. S2).

Evidence for a (μ-Peroxo)Diiron(III) Unit in hDOHH. Fig. 3 shows resonance Raman spectra of different hDOHH samples obtained with 647.1 nm excitation. The spectra of as-isolated and $^{16}O_2$-reoxidized hDOHH ($hDOHH_{16}$) overlay perfectly, indicating that the reoxidized blue species is identical to the as-isolated form (Fig. 3 *A* and *B*). Three features are observed in these spectra at 855 (observed as a Fermi doublet), 493 and 473 cm^{-1}. The combination of these features suggests a diiron(III)-peroxo chromophore, with observed features corresponding to ν(O-O) and ν(Fe-O_2) modes (13, 17, 20). In confirmation, $^{18}O_2$-labeled hDOHH ($hDOHH_{18}$), obtained by exposing $hDOHH_{red}$ to $^{18}O_2$, exhibits features downshifted to 811, 476, and 457 cm^{-1} (Fig. 3*C*), with $\Delta\nu$ values of 44, 17, and 16 cm^{-1}, respectively, that are consistent with those expected for the mass change in the diatomic O-O and Fe-O oscillators (≈50 cm^{-1} and ≈20 cm^{-1}, respectively). From this point on, we designate the blue form of hDOHH as $hDOHH_{peroxo}$.

For the sample prepared by exposing reduced hDOHH to a mixture of 25% $^{16}O_2$, 50% $^{16}O^{18}O$ and 25% $^{18}O_2$ ($hDOHH_M$), a band appears at 833 cm^{-1}, halfway between the ν(O-O) bands in the $hDOHH_{16}$ and $hDOHH_{18}$ spectra, and is assigned to the $^{16}O^{18}O$ isotopomer (Fig. 3*D*). The 3 components of the ν(O-O) band at 856, 833, and 811 cm^{-1} exhibit an intensity ratio consistent with the isotopomer ratio of the mixed-labeled O_2 used. Because of the relatively large (≈20–25 cm^{-1}) width of the individual features, the central component does not show evidence for the presence of distinct $^{16}O^{18}O$ and $^{18}O^{16}O$ isotopomers, as found for oxyhemerythrin (22), but resembles that observed for the mixed-labeled Δ^9D peroxo intermediate (13), which has been assigned as having a symmetric 1,2-O-O bridge. The observations that $hDOHH_{peroxo}$

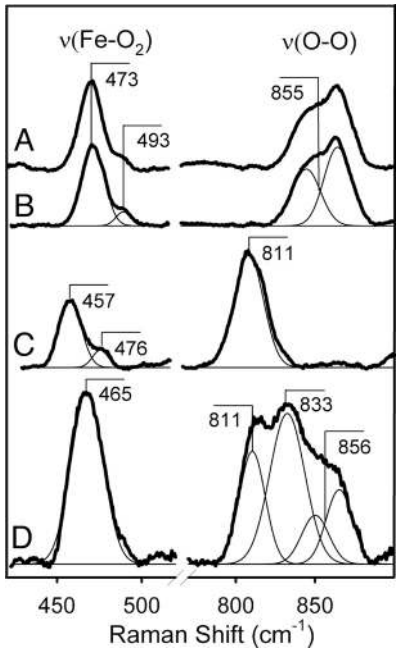

Fig. 3. Resonance Raman spectra of hDOHH samples. (*A*) as-isolated hDOHH. (*B*–*D*) reduced hDOHH exposed to $^{16}O_2$, $^{18}O_2$, and mixed-labeled O_2 ($^{16}O_2$, $^{18}O_2$, and $^{16}O^{18}O$). Background features because of the protein itself have been subtracted using the spectrum of fully reduced hDOHH collected under the same conditions. Experimental data are presented with thick lines and fits are presented with thin lines.

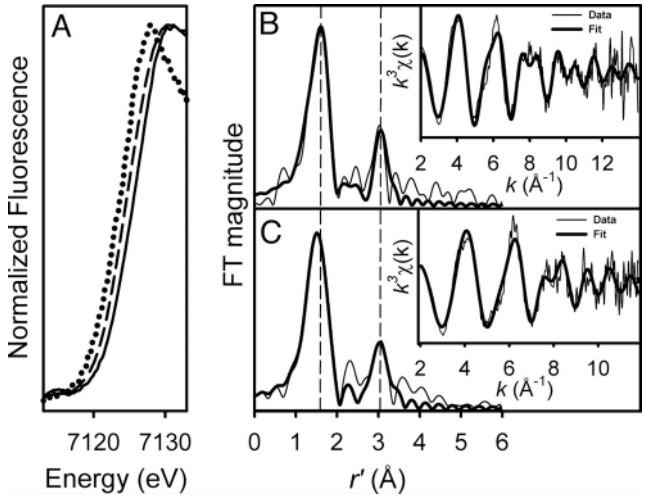

Fig. 4. X-ray absorption spectroscopic analysis of hDOHH. (*A*) XANES spectra of $hDOHH_{peroxo}$ first scans (—), $hDOHH_{phr}$ (– – –), and $hDOHH_{red}$ (···). (*B* and *C*) Fe K-edge EXAFS data $k^3\chi(k)$ of $hDOHH_{phr}$ and $hDOHH_{peroxo}$ and their Fourier transforms (thin lines) in k range = 2–14 $Å^{-1}$ and 2–11.8 $Å^{-1}$, respectively. Best fits are represented by the thick lines. Details of the fitting protocols are provided in Table S1.

has a peroxo-to-iron(III) charge transfer band with λ_{max} of 630 nm and exhibits Raman spectra resembling those of other (μ-1,2-peroxo)diiron(III) centers in proteins and model complexes (Table 1) lead us to propose that the O-O moiety in $hDOHH_{peroxo}$ also bridges the 2 iron atoms in a μ-1,2 mode.

Fig. 4*A* shows X-ray absorption near edge spectra (XANES) of hDOHH. For the as-isolated enzyme, the K-edge energy was observed to downshift from 7126.3 eV in the first scan to 7124.4 eV with increasing exposure to the synchrotron beam, suggesting photoreduction of the sample. The 1.9-eV downshift of the photoreduced sample ($hDOHH_{phr}$) can be compared to the further downshift of 2.0 eV observed in a sample of the dithionite-reduced enzyme (7122.4 eV). This progression suggests that roughly half of the Fe(III) sites in the frozen as-isolated sample in the layer exposed to X-ray beam were reduced to Fe(II), resulting in an edge energy that is the average of the diiron(III) and diiron(II) species. The same stepwise progression has been observed for MMOH as the diiron(III) form was reduced to the diiron(II) form 1 electron at a time (35).

Information about the iron coordination number can be deduced from the intensity of the preedge feature that is attributed to 1s → 3d transitions (36). The preedge areas of 12.0 units for $hDOHH_{peroxo}$ and 13.8 units for $hDOHH_{phr}$ are similar to those of the diiron(III) forms of Δ^9D (≈11−11.5 units) (37), $metHrN_3$ (≈10.4 units), and RNR $R2_{met}$ (10.1 units) but larger than those for the diiron(II,III) form of uteroferrin (4.8 units) (38). The larger preedge areas associated with hDOHH suggest that its iron centers deviate significantly from centrosymmetry with likely coordination numbers of 5.

Because of its superior signal-to-noise ratio we have focused on the analysis of the extended X-ray absorption fine structure (EXAFS) data of $hDOHH_{phr}$ with maximum usable data extending to 14 $Å^{-1}$ (Fig. 4*B*). The Fourier transform of the k^3-weighted EXAFS

Table 1. Properties of diiron(III)-peroxo units in enzymes and related model complexes

Species	λ (nm)	δ (mm/s)	ΔE_Q (mm/s)	J (cm^{-1})	ν(O-O) (cm^{-1})	r(Fe–Fe) (Å)	Ref.
$hDOHH_{peroxo}$	630	0.55, 0.58 (*0.49*, *0.63*)*	1.16, 0.88 (*1.05*, *0.99*)*	50–70	855	3.44	This work
MMOH	725	0.66	1.51				(23)
D84E R2	700	0.63	1.58	50	868	2.50	(15–18, 24)
Δ^9D	700	0.68, 0.64	1.90, 1.06		898		(13, 14)
Frog M Ferritin	650	0.62	1.08	70	851	2.53	(21, 24, 25)
ToMOH	†	0.54	0.66				(26)
OxyHr	500	0.51, 0.54	1.09, 1.92	154	844		(27, 28)
1‡	694	0.66	1.40	66	885	4.01	(29, 30)
2§	600	0.51	0.80	85	900	3.46	(31, 32)
3¶	644	0.50	1.31		908	3.40	(33)
4‖	700 (br)	0.58, 0.65	0.74, 1.70			3.33	(34)

*Mössbauer data can be assigned either to a nested pair of doublets with parameters shown in plain text or to an overlapping pair of doublets with parameters shown in italics.

†No chromophore observed.

‡$[Fe_2(HB(3,5\text{-}iPr_2pz)_3)_2(\mu\text{-}O_2)(\mu\text{-}O_2CCH_2C_6H_5)_2]$ (pz = pyrazole).

§$[Fe_2(N\text{-}Et\text{-}HPTB)(\mu\text{-}O_2)(OPPh_3)_2]^{3+}$ (N-Et-HPTB = anion of *N*,*N*,*N*′,*N*′-tetrakis(1′-ethylbenzimidazolyl-2′-methyl)-2-hydroxy-1,3-diaminopropane).

¶$[Fe_2(6\text{-}Me_2\text{-}BPP)_2(\mu\text{-}O_2)\ (\mu\text{-}OH)]^+$ (6-Me_2-BPP = *N*,*N*-bis(6-methyl-2-pyridylmethyl)-3-aminopropionate).

‖$[Fe_2(Ph\text{-}bimp)(\mu\text{-}O_2)(\mu\text{-}O_2CC_6H_5)]^{2+}$ (Ph-bimp = 2.6-bis[bis{2-(1-methyl-4,5-diphenylimidazolyl)methyl} aminomethyl]-4-methylphenolate).

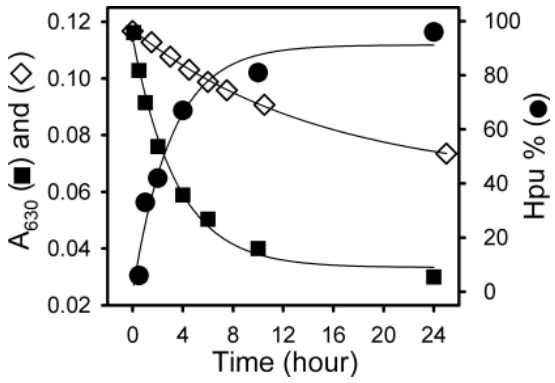

Fig. 5. Reaction of $hDOHH_{peroxo}$ with ≈1 equiv. of substrate, deoxyhypusine-containing eIF5A. The decay of $hDOHH_{peroxo}$ was monitored by following the change in A_{630} at different incubation times in the absence of eIF5A(Dhp) (◇) and in the presence of eIF5A(Dhp) (■). Yields of hypusine (●) are calculated on the basis of the observed amounts of hypusine (Hpu) and deoxyhypusine (Dhp); % Hpu = (Hpu × 100)/(Hpu + Dhp).

data exhibits prominent peaks at 1.6 and 3 Å. The $r' = 1.6$ Å feature of the $hDOHH_{phr}$ data is best fit with 5 O/N scatterers at 2.08 Å, consistent with the preedge analysis. The average iron-ligand bond distance of 2.08 Å is close to those associated with the principal shell of scatterers in the iron(II)iron(III) forms of MMOH (2.06−2.09) (2 histidine/4 carboxylate ligand set) (35) but shorter than the 2.13 Å average distance found in semimetHrN_3 (5 histidine/2 carboxylate ligand set) (39), suggesting a ligand set with more carboxylate ligands than histidines.

The $r' = 3$ Å feature corresponds to an Fe scatterer at 3.44 Å, the addition of which significantly improves the fit quality (compare Fits in bold text in Table S1). This 3.44-Å distance is close to the Fe−Fe distances found in the iron(II)iron(III) sites of photoreduced MMOH (35), uteroferrin (38), and semimetHrN_3 (39). EXAFS analysis thus further corroborates the diiron nature of the active site of $hDOHH_{phr}$.

We have collected first scans on 5 different fresh spots of an as-isolated hDOHH sample, during which photoreduction yield is estimated to be at most ≈25% at $k = 12$ Å^{-1} based on the edge position of the second scans (further details provided in the X-ray absorption spectroscopy section (XAS) in *SI Text*, Figs. S3– S5, and Table S2). The summation of these first scans enables us to carry out a preliminary structural analysis of $hDOHH_{peroxo}$. The best fit to the k^3-weighted EXAFS data of $hDOHH_{peroxo}$ (Table S1) also gives an Fe–Fe distance of 3.44 Å, suggesting that the iron atoms do not move from their original positions upon photoreduction at ≈20 K. Interestingly, the average Fe−O/N distance in the first shell is 2.05 Å, which is 0.03 Å shorter than that for $DOHH_{phr}$, consistent with the change in the diiron oxidation state. The lengthening of the average first-shell distance upon photoreduction without changing the Fe−Fe distance has also been observed in a similar study of MMOH (35).

Long-Lived $hDOHH_{peroxo}$ Can Hydroxylate the Deoxyhypusine Residue in eIF5A. Fig. 5 shows the fate of $hDOHH_{peroxo}$ upon treatment of 1 equivalent (equiv.) of its protein substrate, deoxyhypusine-containing eIF5A [eIF5A(Dhp)]. At room temperature, the absorption at 630 nm of $hDOHH_{peroxo}$, shown above to result from a peroxo-to-iron charge transfer transition, slowly decreases with time. Upon addition of eIF5A(Dhp), the decay rate of A_{630} increases and is comparable to the rate of hypusine formation. After 24 h incubation, deoxyhypusine is almost completely converted to hypusine (≈96%) and $hDOHH_{peroxo}$ turns yellow (Fig. S6). This result indicates that long-lived $hDOHH_{peroxo}$ is activated by substrate binding and carries out the hydroxylation of deoxyhypusine in eIF5A.

Discussion

Our spectroscopic studies have shown that recombinant human DOHH has a nonheme diiron active site, the reduced form of which can react readily with oxygen. This finding extends the family of oxygen-activating nonheme diiron enzymes (10–12, 40) to include for the first time a hydroxylase that is not of bacterial origin and is of vital importance for human metabolism. These nonheme diiron enzymes are capable of carrying out a variety of dioxygen-dependent chemical transformations under mild physiological conditions, including methane hydroxylation by MMO, desaturation of fatty acids by Δ^9D and related desaturases, and the generation of a catalytically essential tyrosyl radical by R2 in DNA biosynthesis (12).

Despite their functional diversity, the diiron enzymes characterized thus far share a common structural motif. The enzymes all have a pair of conserved (D/E)$X_{30-37}EX_2H$ ligand sequence motifs that provide the ligands to a common diiron active site formed within a 4-α-helix bundle (40). hDOHH appears not to follow this pattern. Instead, hDOHH has a pair of conserved $HEX_{31}HE$ sequences that are symmetrically located near the C and N termini, which possibly provide the metal binding ligands (9). On the basis of homology modeling and circular dichroism experiments, the overall structure of hDOHH has been proposed to contain a dyad of 4 consecutive α-hairpins (called a HEAT repeat motif) surrounding the active site (9). Mutagenesis experiments show that both iron binding and activity are lost upon single mutations of the H_n, H_{n+33} and E_{n+34} residues of each $HEX_{31}HE$ sequence to A, but mutation of the E_{n+1} residues to A results in loss of activity but with no loss in iron content (8). These results suggest a 4-His-2-carboxylate ligand set for hDOHH, which is different from the 2-His-4-carboxylate ligand set found in many oxygen-activating diiron enzymes (40). However, EXAFS analysis of hDOHH shows that the average Fe−O/N bond length from the principal shell of ligands to the iron is in fact comparable to those found for diiron enzymes with 2-His-4-carboxylate ligand sets, but shorter than that of the histidine-rich diiron site in hemerythrin (Table S3), so additional experiments are needed to determine which ligands are bound to the diiron site of hDOHH.

In contrast, the accumulated spectroscopic information on hDOHH does shed some light on the nature of its nonprotein-derived ligands. Clearly established is a dioxygen-derived ligand that is identified by resonance Raman experiments to be a peroxide (Fig. 3); this result shows that dioxygen binding to $hDOHH_{red}$ results in the 2e reduction of O_2. Concomitant oxidation of the diiron(II) center to the diiron(III) oxidation state is demonstrated by Mössbauer spectroscopy. The peroxide ligand most likely binds to the diiron(III) center in a 1,2-bridging mode and acts as the principal conduit for the antiferromagnetic interaction (J = 50–70 cm^{-1}) deduced from the analysis of Mössbauer spectra recorded in strong applied magnetic fields. This J value is too small for an oxo bridge ($150 < J < 300$ cm^{-1}) but too large for a hydroxo bridge ($10 < J < 35$ cm^{-1}) (Table 2 of ref. 41). It is in fact comparable to J values found for the (μ-1,2-peroxo)diiron(III) intermediates of RNR W48F/D84E R2 and frog M ferritin (24) and related model (μ-1,2-peroxo)diiron(III) complexes (Table 1).

The Fourier-transformed EXAFS data for $hDOHH_{peroxo}$ and $hDOHH_{phr}$ (Fig. 4) show a strong feature at $r' \approx 3$ Å that corresponds to an Fe scatterer at ≈3.44 Å. The intensity of this peak and the small Debye-Waller factor associated with the Fe scatterer implicate a relatively rigid diiron core structure, which could probably not derive from the presence of the peroxide bridge alone and requires an additional single atom bridge. A perusal of the few synthetic (*cis*-μ-1,2-peroxo)diiron(III) complexes that have been characterized by X-ray crystallography shows that an Fe−Fe distance of 3.4 ± 0.1 Å is associated with

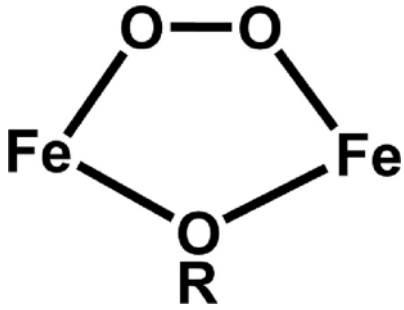

Fig. 6. Proposed core structure of $hDOHH_{peroxo}$

those peroxo complexes with an additional hydroxo or alkoxo bridge (31, 33, 34) (but not an oxo bridge, because it gives rise to shorter Fe−Fe distances of 3.1 ± 0.1 Å , refs. 32, 33). On the basis of these results, we propose the dibridged diiron(III) core structure of $hDOHH_{peroxo}$ shown in Fig. 6.

The 3.44-Å Fe−Fe distance found in $hDOHH_{peroxo}$ stands in distinct contrast to the much shorter 2.5-Å Fe−Fe distances determined by EXAFS for the peroxo intermediates of W48A/D84E R2 (16) and the ferroxidase site of frog M ferritin (21). Such very short metal−metal separations are found only for synthetic complexes that have 2 or 3 single-atom bridges (42, 43). Despite this apparent difference, these 3 diiron(III)-peroxo intermediates exhibit ν(O-O) Raman features of comparable frequency, at 855, 868 (observed for the peroxo intermediate of W48F/D84E R2 and assumed to resemble that of W48A/D84E R2 in structure), and 851 cm^{-1}, respectively (18, 21). The similarity of the ν(O-O) values suggests that the diiron-peroxo core structures may not be as different as suggested by the EXAFS results. This notion derives from a model developed by Brunold and Solomon to rationalize the vibrations of (μ-1,2-peroxo)diiron(III) complexes (44). In this model, the observed ν(O-O) frequency is modulated by mechanical coupling of the O-O and the Fe-O stretching modes, the extent of which is governed by the Fe-O-O angle. As the Fe-O-O angle is related to the Fe−Fe distance, the ν(O-O) can reflect the Fe−Fe distance. This mechanical coupling model is supported by a recent study of a series of synthetic (*cis*-μ-1,2-peroxo)diiron(III) complexes (32). Indeed, a detailed spectroscopic and DFT analysis of the W48F/D84E R2 peroxo intermediate also questions the 2.5-Å Fe−Fe distance deduced by EXAFS and favors an Fe−Fe distance of 3.68 Å (18) that is closer to the 3.44 Å distance we have determined for $hDOHH_{peroxo}$ by EXAFS analysis. On the basis of the calculations, it is proposed that the R2 peroxo intermediate has a (*cis*-μ-1,2-peroxo)diiron(III) center supported by 2 bidentate carboxylate bridges. The absence of a single-atom bridge may rationalize why the predicted Fe scatterer is not observed at 3.7 Å in the EXAFS analysis. There thus appears to be a discrepancy between the Raman and EXAFS results for the peroxo intermediates of D84E R2 and frog M ferritin, which will need to be resolved. For $hDOHH_{peroxo}$, however, the Raman and EXAFS results are in good agreement with respect to the Fe−Fe distance.

Lastly, it is interesting that it is the $hDOHH_{peroxo}$ form that is isolated directly from the expression strain. Its blue chromophore persists for at least several days at room temperature, so its stability surpasses even that of peroxo Δ^9D, the peroxo intermediate obtained from chemically reduced Δ^9D, which has a half-life of ≈30 min at room temperature (14). Thus the lifetimes of diiron-peroxo intermediates of these enzymes vary significantly and can range from milliseconds to days (14–20, 23). Interestingly, the decay of $hDOHH_{peroxo}$ is accelerated by the addition of its substrate, the deoxyhypusine-containing eIF5A. But more remarkable is the observation that the deoxyhypusine residue is in fact hydroxylated to hypusine (Fig. 5). This result implicates $hDOHH_{peroxo}$ as an intermediate on the catalytic pathway of hDOHH.

The extended stability of active $hDOHH_{peroxo}$ raises the questions of what makes it stable and how it is activated. From their studies of W48F/D84E R2, Skulan et al. conclude that a *cis*-μ-1,2-peroxo form is the most stable structure for the diiron(III)-peroxo intermediate and must undergo a structural change before O-O bond cleavage to generate the high valent iron species required for substrate oxidation (18). The additional single-atom bridge deduced to be present in the diiron(III)-peroxo unit in $hDOHH_{peroxo}$ (Fig. 6) is likely to further stabilize the *cis*-μ-1,2-peroxo structure, raising the barrier for O-O bond cleavage to form the high-valent iron oxidant. Indeed a number of metastable synthetic complexes are characterized to have core structures like that shown in Fig. 6; some in fact are stable enough to have been crystallized (31–34). As the target hydroxylation site of hDOHH resides on a protein substrate, it seems plausible that substrate binding triggers a conformation change that activates the (μ-1,2-peroxo)diiron(III) intermediate to carry out eIF5A(Dhp) hydroxylation (Scheme 1). The important role of such protein−protein interactions in modulating enzyme activity has been demonstrated for several diiron enzymes (45–47). As the in vitro reaction of $hDOHH_{peroxo}$ with its protein substrate is very slow, additional protein factors yet to be identified may be required to further accelerate this reaction in the cell.

Materials and Methods

Protein expression and purification was carried out as described previously by Park et al. (8, 9). To prepare ^{57}Fe-hDOHH, ≈10 mg of ^{57}Fe (Cambridge Isotope Laboratories) metal was dissolved in 0.1 mL concentrated H_2SO_4:HNO_3 (3:1) and added to the culture (5 L) at induction. Typical enzyme sample purified by 1-step GSH affinity chromatography is a mixture of ≈30−50% holoenzyme and 50−70% apoenzyme, designated as as-isolated sample.

Reduction and Reoxidation of hDOHH. Sodium dithionite (Sigma-Aldrich) was dissolved in anaerobic buffer, and the concentration was determined using ε_{316} = 8,000 $M^{-1}cm^{-1}$ (48). Protein solutions were made anaerobic in conical vials or in cuvettes sealed with septa by equilibrating under argon atmosphere for 2 h in an ice bath. For tandem reduction-oxidation study, approximately 2.2 equiv. (with respect to diiron cluster) of dithionite was added to the protein solution in a sealed cuvette and the cuvette was opened to introduce oxygen after A_{630} reached a minimum value. For resonance Raman studies, 10 equiv. of dithionite was used, and after complete reduction (judged by UV/Vis spectroscopy) protein samples were equilibrated with anaerobic buffer using 10 K cut-off spin-filters (Pall) in an anaerobic glove box until no dithionite was detected in the flow through solution before exposure to dioxygen sources.

Activity Assay. Approximately 800 μL solution of ≈50 μM $hDOHH_{peroxo}$ and ≈50 μM deoxyhypusine-containing eIF5A in Tris-HCl buffer pH 7.5 was incubated at room temperature for 24 h. At each incubation time a UV/Vis spectrum was collected and 100 μL reaction solution was mixed with 100 μL 20% trichloroacetic acid solution. Self-decay of $hDOHH_{peroxo}$ was monitored under the same conditions but without protein substrate. Hypusine and deoxyhypusine quantification was then carried out as described elsewhere (49).

Spectroscopic Studies. Electron paramagnetic resonance spectroscopy (EPR) spectra were recorded in both perpendicular and parallel modes at X-band and Bruker E500 spectrometer equipped with an Oxford ESR-910 cryostat. Mössbauer spectra were collected with constant acceleration spectrometers, using 2 cryostats that allowed studies at 4.2 K in applied fields up to 8.0 T. Isomer shifts are reported with respect to iron metal at 298 K. The WMOSS software package (WEB Research) was used to analyze the data. Resonance Raman experiments were performed on an Acton AM-506 spectrophotometer (1,200-groove grating) with a Princeton Instruments LN_CCD-1100-PB_UVAR detector cooled to −120 °C with liquid nitrogen. The 647.1 nm excitation line at 100-mW power was provided by a Spectra-Physics BeamLok 2060-KR-RS krypton ion laser, which is filtered out by a Kaiser Optical holographic super notch filter. Samples were contained in flat-bottomed NMR quartz tubes and maintained at a temperature range of −10 °C to 10 °C, and spectra were collected in 90° scattering geometry at resolution of 4 cm^{-1} and referenced to indene. Typically, 256 accumulations of 30-s exposures were collected for each sample. UV/Vis spectra of sample show no change after laser exposure. GRAMS/AI (Thermo Galactic) was used for baseline correction and curve fitting.

X-ray absorption (XAS) data were collected in fluorescence mode on beamline

9–3 at Stanford Synchrotron Radiation Lightsource (SSRL) of the SLAC National Accelerator Laboratory and on beamline X3B at the National Synchrotron Light Source of Brookhaven National Laboratory. Standard procedures were used for data reduction, averaging, processing and EXAFS analysis using EXAFSPAK (50) and FEFF8.40 (51), preedge quantification using SSExafs (52), and XANES linear combination fitting using Athena (53). Additional details on EXAFS data collection and analysis are provided in *SI Text* for X-ray absorption spectroscopy, Figs. S3– S5, S7, and Table S3.

ACKNOWLEDGMENTS. This work was supported in part by the Intramural Research Program of the National Institute of Dental and Craniofacial Research, National Institutes of Health (NIH), and by NIH Grants GM38767 (to L.Q.) and EB-001475 (to E.M.) and a Vietnam Education Foundation Fellowship (to V.V.V.). XAS data were collected on Beamline X3B at the National Synchrotron Radiation Light Source and Beamline 9–3 at the Stanford Synchrotron Radiation Lightsource, both of which are supported by the U.S. Department of Energy and NIH. We thank Mr. Erik R. Farquhar and Mr. Jonathan R. Frisch for experimental and writing assistance.

1. Park MH (2006) The post-translational synthesis of a polyamine-derived amino acid, hypusine, in the eukaryotic translation initiation factor 5A (eIF5A). *J Biochem* 139:161–169.
2. Wolff EC, Kang KR, Kim YS, Park MH (2007) Posttranslational synthesis of hypusine: Evolutionary progression and specificity of the hypusine modification. *Amino Acids* 33:341–350.
3. Byers TL, Lakanen JR, Coward JK, Pegg AE (1994) The role of hypusine depletion in cytostasis induced by S-adenosyl-L-methionine dercarboxylase inhibition: New evidence provided by 1-methylspermidine and 1,12-dimethylspermidine. *Biochem J* 303:363–368.
4. Park MH, Wolff EC, Leea YB, Folk JE (1994) Antiproliferative effects of inhibitors of deoxyhypusine synthase: Inhibition of growth of Chinese hamster ovary cells by guanul diamines. *J Biol Chem* 269:27827–27832.
5. Hanauske-Abel HM, et al. (1994) Inhibition of the G1-S transition of the cell cycle by inhibitors of deoxyhypusine hydroxylation. *Biochim Biophys Acta* 1221:115–124.
6. Clement PMJ, Hanauske-Abel HM, Wolff EC, Kleinman HK, Park MH (2002) The antifungal drug ciclopirox inhibits deoxyhypusine and proline hydroxylation, endothelial cell growth and angiogenesis *in vitro*. *Int J Cancer* 100:491–498.
7. Andrus L, et al. (1998) Antiretroviral effects of deoxyhypusyl hydroxylase Inhibitors: A hypusine-dependent host cell mechanism for replication of human immunodeficiency virus type 1 (HIV-1). *Biochem Pharmacol* 55:1807–1818.
8. Kim YS, et al. (2006) Deoxyhypusine hydroxylase is a Fe(II)-dependent, HEAT-repeat enzyme. Identification of amino acid residues critical for Fe(II) binding catalysis. *J Biol Chem* 281:13217–13225.
9. Park J-H, et al. (2006) Molecular cloning, expression, and structural prediction of deoxyhypusine hydroxylase: A HEAT-repeat-containing metalloenzyme. *Proc Natl Acad Sci USA* 103:51–56.
10. Notomista E, Lahm A, Di Donato A, Tramontano A (2003) Evolution of bacterial and archaeal multicomponent monooxygenases. *J Mol Evol* 56:435–445.
11. Leahy JG, Batchelor PJ, Morcomb SM (2003) Evolution of the soluble diiron monooxygenases. *FEMS Microbiol Rev* 27:449–479.
12. Wallar BJ, Lipscomb JD (1996) Dioxygen activation by enzymes containing binuclear non-heme iron clusters. *Chem Rev* 96:2625–2657.
13. Broadwater JA, Ai J, Loehr TM, Sanders-Loehr JS, Fox BG (1998) Peroxodiferric intermediate of stearoyl-acyl carrier protein Δ^9 desaturase: Oxidase reactivity during single turnover and implications for the mechanism of desaturation. *Biochemistry* 37:14664–14671.
14. Broadwater JA, Achim C, Münck E, Fox BG (1999) Mössbauer studies of the formation and reactivity of a quasi-stable peroxo intermediate of stearoyl-acyl carrier protein Δ^9-desaturase. *Biochemistry* 38:12197–12204.
15. Bollinger JM, Jr, et al. (1998) Engineering the diiron site of *Escherichia coli* ribonucleotide reductase protein R2 to accumulate an intermediate similar to H_{peroxo}, the putative peroxodiiron(III) complex from the methane monooxygenase catalytic cycle. *J Am Chem Soc* 120:1094–1095.
16. Baldwin J, et al. (2003) Structural characterization of the peroxodiiron(III) intermediate generated during oxygen activation by the W48A/D84E variant of ribonucleotide reductase protein R2 from *Escherichia coli*. *Biochemistry* 42:13269–13279.
17. Moenne-Loccoz P, Baldwin J, Ley BA, Loehr TM, Bollinger JM, Jr (1998) O_2 activation by non-heme diiron proteins: Identification of a symmetric μ-1,2-peroxide in a mutant of ribonucleotide reductase. *Biochemistry* 37:14659–14663.
18. Skulan AJ, et al. (2004) Nature of the peroxo intermediate of the W48F/D84E ribonucleotide reductase variant: Implications for O_2 activation by binuclear non-heme iron enzymes. *J Am Chem Soc* 126:8842–8855.
19. Yun D, et al. (2007) (μ-1,2-peroxo)diiron(III/III) complex as a precursor to the diiron(III/IV) intermediate X in the assembly of the iron-radical cofactor of ribonucleotide reductase from mouse. *Biochemistry* 46:1925–1932.
20. Moenne-Loccoz P, et al. (1999) The ferroxidase reaction of ferritin reveals a diferric μ-1,2 bridging peroxide intermediate in common with other O_2-activating non-heme diiron proteins. *Biochemistry* 38:5290–5295.
21. Hwang J, et al. (2000) A short Fe-Fe distance in peroxodiferric ferritin: Control of Fe substrate versus cofactor decay? *Science* 287:122–125.
22. Kurtz DM, Jr, Shriver DF, Klotz IM (1976) Resonance Raman spectroscopy with unsymmetrically isotopica ligands. Differentiation of possible structures of hemerythrin complexes. *J Am Chem Soc* 98:5033–5035.
23. Liu KE, et al. (1995) Characterization of a diiron(III) peroxide intermediate in the reaction cycle of methane monooxygenase hydroxylase from *Methylococcus capsulatus* (Bath). *J Am Chem Soc* 117:4997–4998.
24. Krebs C, Bollinger JM, Jr, Theil EC, Huynh BH (2002) Exchange coupling constant J of peroxodiferric reaction intermediates determined by Mössbauer spectroscopy. *J Biol Inorg Chem* 7:863–869.
25. Pereira AS, et al. (1998) Direct spectroscopic and kinetic evidence for the involvement of a peroxodiferric intermediate during the ferroxidase reaction in fast ferritin mineralization. *Biochemistry* 37:9871–9876.
26. Murray LJ, Garcia-Serres R, Naik S, Huynh BH, Lippard SJ (2006) Dioxygen activation at non-heme diiron centers: Characterization of intermediates in a mutant form of toluene/*o*-xylene monooxygenase hydroxylase. *J Am Chem Soc* 128:7458–7459.
27. Okamura MY, Klotz IM, Johnson CE, Winter MRC, Williams RJP (1969) The state of iron in hemerythrin. A Mössbauer study. *Biochemistry* 8:1951–1958.
28. Dawson JW, et al. (1972) A magnetic susceptibility study of hemerythrin using an ultrasensitive magnetometer. *Biochemistry* 11:461–465.
29. Kitajima N, et al. (1994) Monomeric carboxylate ferrous complexes as models for the dioxygen binding sites in non-heme iron proteins. The reversible formation and characterization of μ-peroxo diferric complexes. *J Am Chem Soc* 116:9071–9085.
30. Kim K, Lippard SJ (1996) Structure and Mössbauer spectrum of a (μ-1,2-peroxo)bis(μ-carboxylato)diiron(III) model for the peroxo intermediate in the methane monooxygenase hydroxylase reaction cycle. *J Am Chem Soc* 118:4914–4915.
31. Dong Y, Yan S, Young VG, Jr, Que L, Jr (1996) Crystal structure analysis of a synthetic non-heme diiron-O_2 adduct: Insight into the mechanism of oxygen activation. *Angew Chem Int Ed (Engl)* 35:618–620.
32. Fiedler AT, et al. (2008) Spectroscopic and computational studies of (μ-Oxo)(μ-1,2-peroxo)diiron(III) complexes of relevance to nonheme diiron oxygenase intermediates. *J Phys Chem A* 112:13037–13044.
33. Zhang X, et al. (2005) Structural and spectroscopic characterization of (μ-hydroxo or μ-oxo)(μ-peroxo)diiron(III) complexes: Models for peroxo intermediates of non-heme diiron proteins. *J Am Chem Soc* 127:826–827.
34. Ookubo T, et al. (1996) cis-μ-1,2-peroxo diiron complex: Structure and reversible oxygenation. *J Am Chem Soc* 118:701–702.
35. DeWitt JG, et al. (1991) X-ray absorption, Mössbauer, and EPR studies of the dinuclear iron center in the hydroxylase component of methane monooxygenase. *J Am Chem Soc* 113:9219–9235.
36. Roe AL, et al. (1984) X-ray absorption spectroscopy of iron-tyrosinate proteins. *J Am Chem Soc* 106:1676–1681.
37. Shu L, et al. (1998) EXAFS and Mössbauer characterization of the diiron(III) site in stearoyl-acyl carrier protein Δ^9-desaturase. *J Biol Inorg Chem* 3:392–400.
38. True AE, Scarrow RC, Randall CR, Holz RC, Que L, Jr (1993) EXAFS studies of uteroferrin and its anion complexes. *J Am Chem Soc* 115:4246–4255.
39. Scarrow RC, et al. (1987) EXAFS studies of binuclear iron proteins: Hemerythrin and ribonucleotide reductase. *J Am Chem Soc* 109:7857–7864.
40. Kurtz DM, Jr (1997) Structural similarity and functional diversity in diiron-oxo proteins. *J Biol Inorg Chem* 2:159–167.
41. Kurtz DM, Jr (1990) Oxo- and hydroxo-bridged diiron complexes: A chemical perspective on a biological unit. *Chem Rev* 90:585–606.
42. Bossek U, Weyhermueller T, Wieghardt K, Nuber B, Weiss J (1990) $[L_2Mn_2(\mu\text{-}O)_2(\mu\text{-}O_2)](ClO_4)_2$. The first binuclear ($\mu$-peroxo)dimanganese(IV) complex (L = 1,4,7-trimethyl-1,4,7-triazacyclononane). A model for the $S_4 \rightarrow S_0$ transformation in the oxygen-evolving complex in photosynthesis. *J Am Chem Soc* 112:6387–6388.
43. Gamelin DR, Bominaar EL, Kirk ML, Wieghardt K, Solomon EI (1996) Excited-state contributions to ground-state properties of mixed-valence dimers: Spectral and electronic-structural studies of $[Fe_2(OH)_3(tmtacn)_2]^{2+}$ related to the $[Fe_2S_2]^+$ active sites of plant-type ferredoxins. *J Am Chem Soc* 118:8085–8097.
44. Brunold TC, Tamura N, Kitajima N, Moro-oka Y, Solomon EI (1998) Spectroscopic study of $[Fe_2(O_2)(OBz)_2\{HB(pz')_3\}_2]$: Nature of the μ-1,2 peroxide-Fe(III) bond and its possible relevance to O_2 activation by non-heme iron enzymes. *J Am Chem Soc* 120:5674–5690.
45. Liu Y, Nesheim JC, Lee S-K, Lipscomb JD (1995) Gating effects of component B on oxygen activation by the methane monooxygenase hydroxylase component. *J Biol Chem* 270:24662–24665.
46. Bailey LJ, McCoy JG, Phillips GN, Fox BG (2008) Structural consequences of effector protein complex formation in a diiron hydroxylase. *Proc Natl Acad Sci USA* 105:19194–19198.
47. Fox BG, Lyle KS, Rogge CE (2004) Reactions of the diiron enzyme stearoyl-acyl carrier protein desaturase. *Acc Chem Res* 37:421–429.
48. Dixon M (1971) The acceptor specificity of flavins and flavoproteins. I. Techniques for anaerobic spectrophotometry. *Biochim Biophys Acta* 226:241–258.
49. Park MH, Cooperg HL, Folk JE (1982) The biosynthesis of hypusine (N^{ε}-(4-amino-2-hydroxybutyl)lysine): Lysine as the amino acid precursor and the intermediate role of deoxyhypusine (N^{ε}-(4-aminobutyl)lysine). *J Biol Chem* 259:7217–7222.
50. George GN, Pickering IJ (2000) *EXAFSPAK and EDGFIT*. (Stanford Synchrotron Radiation Laboratory, Stanford Linear Accelerator Center, Stanford University, Stanford, CA).
51. Rehr JJ, Mustre de Leon J, Zabinsky SI, Albers RC (1991) Theoretical x-ray absorption fine structure standards. *J Am Chem Soc* 113:5135–5140.
52. Scarrow RC, et al. (1994) X-ray spectroscopy of the iron site in soybean lipoxygenase-1: Changes in coordination upon oxidation or addition of methanol. *Biochemistry* 33:15023–15035.
53. Ravel B, Newville M (2005) ATHENA, ARTEMIS, HEPHAESTUS: Data analysis for X-ray absorption spectroscopy using IFEFFIT. *J Synchrotron Rad* 12:537–541.